

HYDROELASTIC RESPONSE OF VLFS ON UNEVEN SEA BOTTOM

Hao Song

School of Engineering, Griffith University, PMB50 GCMC,
Gold Coast, QLD, 9726, Australia

Longbin Tao

School of Engineering, Griffith University, PMB50 GCMC,
Gold Coast, QLD, 9726, Australia

Weicheng Cui

China Ship Scientific Research Centre, Wuxi, 214082, China

Yingzhong Liu

School of Naval Architecture, Ocean and Civil Engineering,
Shanghai Jiao Tong University, Shanghai, 200030, China

ABSTRACT

Hydroelastic response of VLFS under inhomogeneous sea environment is an important issue in offshore engineering applications. The most typical inhomogeneous ocean environment in offshore engineering is the inhomogeneity caused by the uneven sea bottom. In this paper, the hydroelastic response of VLFS due to the variation of water depth is studied experimentally and numerically. Experiments were performed in the state key laboratory of ocean engineering at Shanghai Jiao Tong University (SJTU). Different shoals were set on the bottom of the wave basin to simulate the uneven sea bottom. The cases tested in the Lab were studied by extending the traditional hydroelastic method in constant water depth to the varied water depth. Comparisons between the experimental measurements and the numerical results show good agreement. It is found that the inhomogeneous ocean environment has some effect on the hydroelastic response of VLFS.

INTRODUCTION

Many studies have been carried out for the prediction of the hydroelastic responses of VLFSs. However, in most of these studies, the offshore environment around a VLFS is assumed to be homogeneous, such as uniform incoming waves and even sea bottom. As a matter of fact, environment at one end of the VLFS may be different from that at the other end of several kilometres away (Bai et al., 1999; Webster, 2000). Although it was pointed out more than 10 years ago in the discussion of the first VLFS workshop (VLFS'91), to date, the impact of the inhomogeneous environment on the hydroelastic response of a VLFS is still not well understood and only a few references could be found (Utsunomiya et al., 2001; Takagi & Kohara, 2000; Wang & Meylan, 2002).

There are two types of independent inhomogeneities: one is due to the variation of the fixed boundary conditions such as variations of sea bottom and coastlines; another is due to the variation of instant conditions such as wind and waves. Most

mat-like VLFSs are constructed in near shore area where the sea bottom has more variations than in open seas. In this paper, hydroelastic model tests over different shoals were carried out in the state key laboratory of ocean engineering of Shanghai Jiao Tong University (SJTU) to study the hydroelastic response of VLFS due to the variation of water depth. The model and shoals are designed based on the law of similitude. The traditional hydroelasticity method for constant water depth is extended to the varied water depth in straightforward manner. The results from both experimental and numerical simulation are presented, followed with the discussion on the importance of the uneven sea bottom on the hydroelastic response of a VLFS based on the present results.

EXPERIMENTAL CAMPAIGN

Model tests on a 1:100 model of a VLFS in regular waves were conducted at the Offshore Wave Basin, Shanghai Jiao Tong University, China. The ocean engineering basin is 50m in length, 30m in width and 6m in depth. Various ocean environments can be simulated by a powerful hydraulic wave maker of dual-flap type and a large area moveable bottom (28m×26m). Both regular and irregular long crest waves can be generated with the maximum wave height up to 0.6m. And the water depth can be adjusted between 0 and 5m. The primary objective of the tests is to obtain the hydroelastic response of a VLFS on even and uneven sea bottom. The prototype of the VLFS was constructed by the Technological Research Association of Mega-Float (Phase II) in Japan in 1999 (Isobe, 1999; Miyajima et al., 2002). The principal particulars of model and its prototype are given in Table 1. Three configurations of shoal models comprising of different length, breadth and height were considered in the study (Table 2).

Figure 1 shows the sketch of shoal models on sea bottom. 2D shoal is an elliptical column and 10 times longer than the width of VLFS model. The water depth is considered a 2D variation in this situation. 3D shoal is a part of an elliptical

sphere. Figure 2 shows models in the test. The wavelengths of the incoming waves are 0.5m, 1m, 2m and 4m respectively. The water depths are 0.2m, 0.4m and 0.6m respectively. The wave height is 0.02m and the wave directions are 0°, 30° and 60° respectively.

Table 1 Principal particular of the VLFS model and prototype

	Prototype	Model
Length	1000m	10m
Breadth	60m (partly 121m)	0.6m
Depth	3m	0.03m
Draft	1m	0.01m
Stiffness EI	About $1.11 \times 10^{12} \text{N.m}^2$	125.73 N.m ²

Table 2 Test matrix for the experimental and numerical study

Type	No.	Length (ls)	Breadth of section (bs)	Height of section (hs)
2D	A	6.0m	1.0m	0.1m
2D	B	6.0m	2.0m	0.1m
3D	C	2.0m	2.0m	0.1m

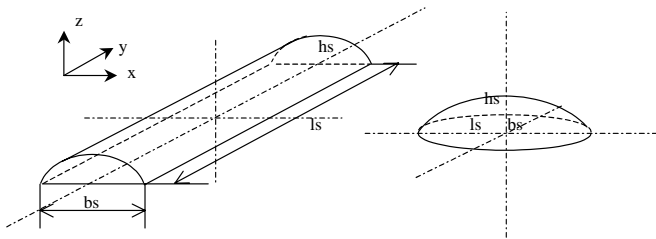


Figure 1 The sketch of shoal models



(a) Model on 2D shoal



(b) Model on 3D shoal

Figure 2 Models in the test

NUMERICAL METHOD

A thin elastic rectangular plate representing a floating mat-like VLFS, with length L , breadth B and thickness T , is considered. As shown in Figure 3, the calm water surface is designated as the x, y plane with positive z axis pointing upwards. Region II ($0 \leq x \leq L, 0 \leq y \leq B$) is covered by plate while region I is the fluid region. The plate is freely floating on an ideal fluid layer of variable depth $h(x, y)$, and is under the action of linear water waves of frequency ω and direction θ . The two regions are separated by the juncture boundary J .

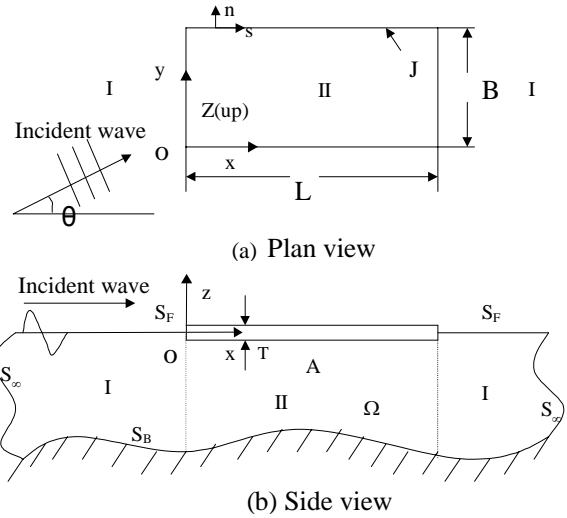


Figure 3 Definition of the problem

Assumed that the relative variation of the gradient of the sea bottom is small, the problem can be described within the scope of the linear theory as follows:

For fluid, one has:

$$\left(\frac{\partial^2}{\partial x^2} + \frac{\partial^2}{\partial y^2} + \frac{\partial^2}{\partial z^2}\right)\Phi = 0 \quad (\text{in I, II}) \quad (1)$$

$$g \frac{\partial \Phi}{\partial z} + \frac{\partial^3 \Phi}{\partial t^2} = 0 \quad \text{on } z = \zeta(x, y) \quad (\text{in I}) \quad (2)$$

$$\frac{\partial \Phi}{\partial z} = \frac{\partial w}{\partial t} \quad \text{on } A \quad (\text{in II}) \quad (3)$$

$$\frac{\partial \Phi}{\partial n} = 0 \quad \text{on } z = -h(x, y) \quad (\text{in I, II}) \quad (4)$$

For plate,

$$DV^4 w + \rho g w + m \frac{\partial^2 w}{\partial t^2} = -\rho \frac{\partial \Phi}{\partial t} \quad (5)$$

$$\frac{\partial^2 w}{\partial x^2} + \nu \frac{\partial^2 w}{\partial y^2} = 0 \quad \frac{\partial^3 w}{\partial x^3} + (2 - \nu) \frac{\partial^3 w}{\partial y^2 \partial x} = 0 \quad (x = 0, L) \quad (6)$$

$$\nu \frac{\partial^2 w}{\partial x^2} + \frac{\partial^2 w}{\partial y^2} = 0 \quad \frac{\partial^3 w}{\partial y^3} + (2 - \nu) \frac{\partial^3 w}{\partial y \partial x^2} = 0 \quad (y = 0, B) \quad (7)$$

$$\frac{\partial^2 w}{\partial x \partial y} = 0 \quad (x = 0, L), (y = 0, B) \quad (8)$$

where Φ is velocity potential, w is the deflection of plate, ζ is the wave height, A is the interface of fluid and structure, ν is the Poisson's ratio, ρ is the mass density of the plate, g is the gravitational acceleration, m is the mass per unit area, and n is the unit normal vector.

The velocity potential can be decomposed as the sum of incident non-uniform wave potential, the scattering potential and the radiation potential due to the motion and deflection of the plate, i.e.

$$\Phi = \Phi_I + \Phi_S + \Phi_R \quad (9)$$

The incoming wave is:

$$\Phi_I = \frac{iga \cosh[k_0(z+h_0)]}{\omega \cosh(k_0 h_0)} e^{[-i(k_p x \cos \theta + k_0 y \sin \theta) + i\omega t]} \quad (10)$$

$$\zeta_0 = a e^{[-i(k_p x \cos \theta + k_0 y \sin \theta) + i\omega t]} \quad (11)$$

where a is the amplitude of incoming wave, k is the wave number, h_0 and k_0 are constant water depth and wave number respectively in even bottom zone from $x = -\infty$.

For scatter potential and radiation potential, one has:

$$\frac{\partial \Phi_S}{\partial z} = -\frac{\partial \Phi_I}{\partial z} \quad \text{on } A \quad (\text{in II}) \quad (12)$$

$$\frac{\partial \Phi_R}{\partial z} = \frac{\partial w}{\partial t} \quad \text{on } A \quad (\text{in II}) \quad (13)$$

Within the scope of the linear theory, the motions of the plate and fluid can be assumed to be time harmonic with the same frequency ω of the incoming waves. Let us define

$$\begin{aligned} \Phi(x, y, z, t) &= \phi(x, y, z) e^{i\omega t} \\ \Phi_I(x, y, z, t) &= \phi_I(x, y, z) e^{i\omega t} \\ w(x, y, z, t) &= w(x, y, z) e^{i\omega t} \end{aligned} \quad (14)$$

By introducing a plate Green function $g_p(x, x'; y, y')$ which is defined by the following equations (Taylor & Ohkusu, 2000; Yan, et al., 2003):

$$(\rho g - m\omega^2)g_p + D\left(\frac{\partial^4 g_p}{\partial x^4} + 2\frac{\partial^4 g_p}{\partial x^2 \partial y^2} + \frac{\partial^4 g_p}{\partial y^4}\right) = \delta(x, x'; y, y')$$

$$\frac{\partial^2 g_p}{\partial n^2} + \nu \frac{\partial^2 g_p}{\partial s^2} = 0, \quad \frac{\partial^3 g_p}{\partial n^3} + (2-\nu) \frac{\partial^3 g_p}{\partial n \partial s^2} = 0 \quad \text{on } J \quad (15)$$

The solution for deflection can be written in the following form:

$$w = \iint_A -i\omega \rho \phi g_p dS \quad (16)$$

Let us define

$$\phi_s = \phi - \phi_I \quad (17)$$

For ϕ_s :

$$\begin{cases} \nabla^2 \phi_s = 0 & \text{in } \Omega \\ \frac{\partial \phi_s}{\partial z} = \frac{\omega^2}{g} \phi_s & \text{on } S_F \\ \frac{\partial \phi_s}{\partial n} = 0 & \text{on } S_B \\ \lim_{R \rightarrow \infty} \sqrt{R} \left[\frac{\partial \phi_s}{\partial R} + ik \phi_s \right] = 0 & \text{on } S_\infty \end{cases} \quad (18)$$

From Wu (1984), the fluid Green function can be taken as the following series form:

$$\begin{aligned} G_f &= \frac{2\pi(\nu^2 - k^2)}{(k^2 - \nu^2)h + \nu} \cosh k(z+h) \cosh k(\zeta+h) [Y_0(kR) + iJ_0(kR)] \\ &+ 4 \sum_{m=1}^{\infty} \frac{\mu_m^2 + \nu^2}{(\mu_m^2 + \nu^2)h - \nu} \cos \mu_m(\zeta+h) \cos \mu_m(z+h) K_0(\mu_m R) \end{aligned} \quad (19)$$

where,

$$\begin{aligned} R &= \sqrt{(x-\xi)^2 + (y-\eta)^2} \\ \nu &= \frac{\omega^2}{g} = k \tanh(kh) \end{aligned} \quad (20)$$

μ_m denotes the positive root of $\mu_m \tan \mu_m h + \nu = 0$

If ϕ_s and G_f are any two functions which, together with their first and second order derivatives are finite and single valued throughout a given fluid domain Ω enclosed by the surface $S=S_\infty+S_F+S_B+A$, then the Green's second identity shows that

$$\begin{aligned} -2\pi \cdot \phi_s &= \iint_A \left(\phi_s \frac{\partial G_f}{\partial z} - G_f \frac{\partial \phi_s}{\partial z} \right) dS + \iint_{S_\infty} \left(\phi_s \frac{\partial G_f}{\partial n} - G_f \frac{\partial \phi_s}{\partial n} \right) dS \\ &+ \iint_{S_B} \left(\phi_s \frac{\partial G_f}{\partial n} - G_f \frac{\partial \phi_s}{\partial n} \right) dS + \iint_{S_F} \left(\phi_s \frac{\partial G_f}{\partial z} - G_f \frac{\partial \phi_s}{\partial z} \right) dS \end{aligned} \quad (21)$$

For the case shown in Figure 3, the problem can be simplified as follows:

$$-2\pi \cdot (\phi - \phi_I) = \iint_{A+S_B} \phi \frac{\partial G_f}{\partial n} dS - \iint_A G_f \frac{\partial \phi}{\partial n} dS - \iint_{S_B} \phi_I \frac{\partial G_f}{\partial n} dS \quad (22)$$

Using Eq.(16), we obtain

$$\begin{aligned} -2\pi \cdot (\phi - \phi_I) &= -\omega^2 \iint_A \left[\rho \iint_A \phi g_p dS' - \frac{\phi}{g} \right] G_f dS \\ &+ \iint_{S_B} (\phi - \phi_I) \frac{\partial G_f}{\partial n} dS \end{aligned} \quad (23)$$

The equation can be solved by Boundary Element Method (BEM). The deflection of plate is then obtained by solving Eq.(16). It is noticed that S_B is a curve plane. The following form of $g_p(x, x'; y, y')$ suggested by (Taylor & Ohkusu, 2000) is adopted in the present numerical computation:

$$w = c_0 + c_1x + c_2y + c_3xy + \sum_{m=1}^M [u_{0m}(1-y) + u_{1m}y] \sin m\pi x + \sum_{n=1}^N [v_{0n}(1-x) + v_{1n}x] \sin n\pi y + \sum_{m=1}^M \sum_{n=1}^N P_{mn} \sin m\pi x \sin n\pi y \quad (24)$$

RESULTS AND DISCUSSION

First, let us compare the results of the deflection amplitudes along the centreline of the VLFS on even bottom between experimental data and numerical computation. All the results presented here are for prototype VLFS. Four different wavelengths ($\lambda=50\text{m}$, 100m , 200m , 400m), three different water depths ($h=20\text{m}$, 40m , 60m) and three incident wave angles ($\theta=0^\circ$, 30° , 60°) are shown in Figure 4 where circles denote the experimental data. It is found that the numerical results are in good agreement with the experimental measurements for all cases of even sea bottom tested in the study. It is seen that the effect of wavelength on the plate deflection is limited when λ/L is small. However, as can be seen from the figure, the plate deflection significantly increases as wavelength continue to increase ($\lambda=200\text{m}$). Figure 4 also shows that the effect of water depth on the plate deflection at even sea bottom is weak. The most striking effect of the wave properties on the hydroelastic response on even bottom appears to be the incident wave angles. It is observed from Figure 4 that the deflections of the plate increases significantly as incident wave angle increases indicating that considerable larger deflections in oblique waves than that in head seas.

Figures 5~7 show the deflection amplitudes along the centreline between the experimental data and numerical results of the VLFS on uneven bottoms A, B and C respectively. The centres of VLFS and the shoal coincide with each other. Longitudinal centreline of the VLFS is perpendicular to the shoal. All cases shown in the figures are in head seas. The last two cases in Figures 5 and 6 are the results when the position of shoal is moved forward with distance $L/4$ and $L/4-b_s/2$, where L is the length of VLFS and b_s is the breadth of the shoal. The last two cases in Figures 7 are the results when the position of shoal is moved forward and left with $(L/4, 0)$ and $(L/4, B/2)$, where B is the breadth of VLFS. The values of X_m in Figure 5~7 represent the distances of the shoal moved forward from the centre location and the values of Y_m in Figure 7 represent the distances of the shoal moved leftward from the centre location. As can be seen from the Figures, reasonably good agreement is achieved between the results obtained by numerical computation and experimental measurements. This further demonstrates that the numerical method described in previous section can be used to predict the hydroelastic response of VLFS on uneven bottom. It is noted that some discrepancy is also observed in Figures corresponding to the cases of large wavelength. As λ increases, Ursell number ($U_r = A_w / h / (kh)^2 = A_w \lambda^2 / h^3 (2\pi)^2$, where A_w is the amplitude of wave) will be greater than 1 over the uneven bottom. The problem becomes nonlinear, and as a consequence of that, the present numerical method based on linear theory is no longer applicable. It is noteworthy that the calculations are rather time consuming. To make the figures legible, the following discussions on the effects of various factors on the

hydroelastic responses of VLFS on uneven bottom are based on the experimental results.

Figure 8 shows the experimental results of the plate deflection of four different wavelengths under four different bottom configurations A, B, C and even bottom respectively. The centres of the shoal are located at the middle of the VLFS. It can be seen that as wavelength increases, the plate deflection also increases for all three uneven bottom configurations, and the deflection tends to be non-uniform along the longitudinal centreline of the VLFS, compared with the even bottom case. The effect of water depth on the plate deflection is shown in Figure 9. It is clearly seen that the plate deflection appeared very large at the forepart and decreases along the longitudinal centreline. The curve of the smallest water depth ($h=20\text{m}$) is appeared to be oscillating with large amplitude while the much smoother curves of larger water depths ($h=40\text{m}$, 60m) and very close to each other are observed. Figure 9 also indicates that the effect of water depth on hydroelastic response decreases as water depth increases. In order to examine the effect of shoal position on the hydroelastic response of VLFS, a series model tests are carried out for the three shoal models being placed at different locations. The results of the plate deflection are shown in Figure 10. As the shoal is placed at the centre of VLFS, it is seen that the deflection of forepart of VLFS is almost identical to that of even sea bottom. At $X/L \approx 0.2$, the deflections of the plate begin to oscillate at different frequencies indicating the presence of the shoal, and differences of the deflection persist to the back end. Similar results for shoal moved a distance of $X_m=(L/4-b_s/2)$ and $X_m=L/4$ are also observed with the deflection of rear part varying mildly. This demonstrates that, under the wave conditions tested, the impact of the inhomogeneous environment in the form of uneven sea bottom is limited to the surrounding area and down stream. When the position of shoal is moved aside, the deflection of the longitudinal centreline of VLFS decreases at its downstream of the location of the shoal.

Figure 11 shows the effects of wavelength and different bottoms on the deflection of VLFS in inhomogeneous environment. The water depth is 20m for all cases shown in Figure 11. As can be seen from the figure, when the incoming wave is very short, $\lambda=50\text{m}$, the deflection of VLFS is relatively low except at both ends of the plate. The deflections on different shoals have less difference. When the wavelength increases, a non-uniform pattern of the deflection along the longitudinal centreline becomes obvious due to the effect of inhomogeneity condition at the sea bottom. The responses of VLFS on shoal B and C with relatively low surface gradient are significantly higher than shoal A and even bottom ($\lambda=200\text{m}$). As the wavelength continue to increase, e.g., $\lambda=400\text{m}$ as shown in the figure, the response of VLFS on even bottom appears to be greater than all the uneven sea bottom configurations tested in this study.

The effects of incident wave angle on the deflection of VLFS on shoal C and even bottom are shown in Figure 12. It is found that when the incident wave angle increases, the deflection of VLFS also increases but the effect of the variation of bottom is weakened.

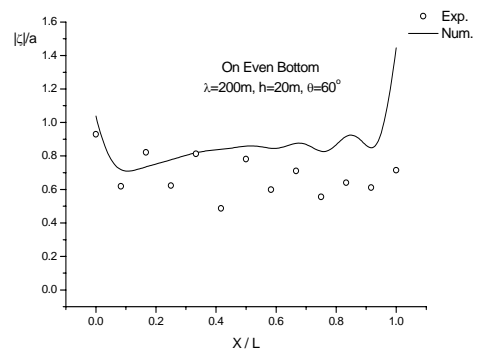
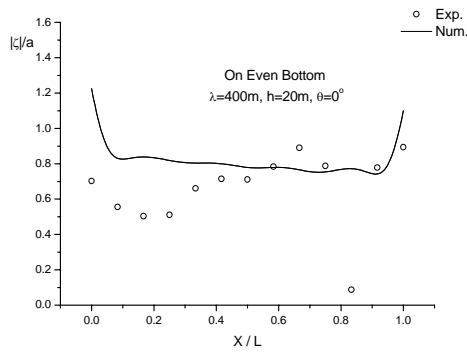
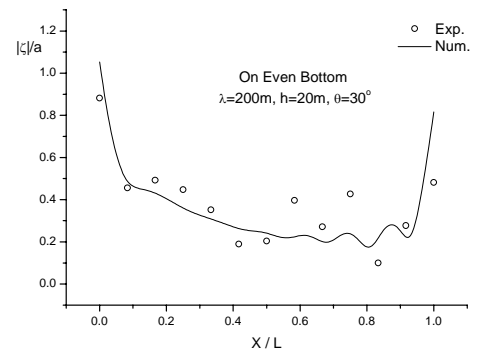
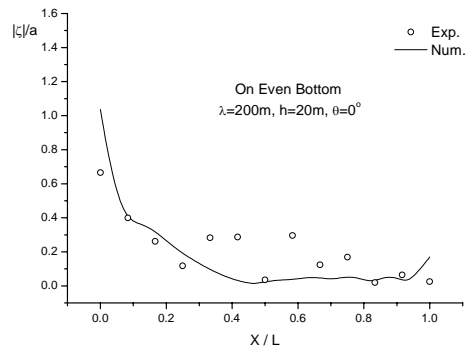
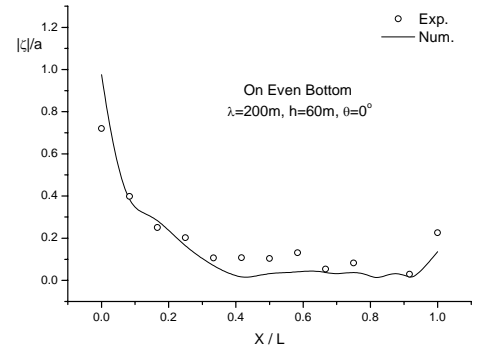
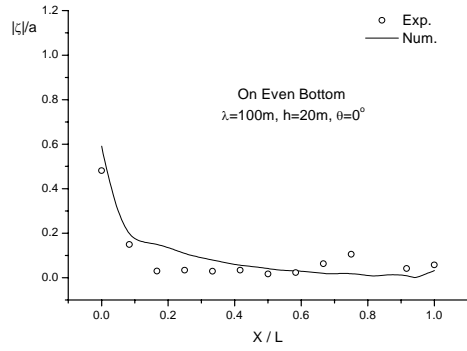
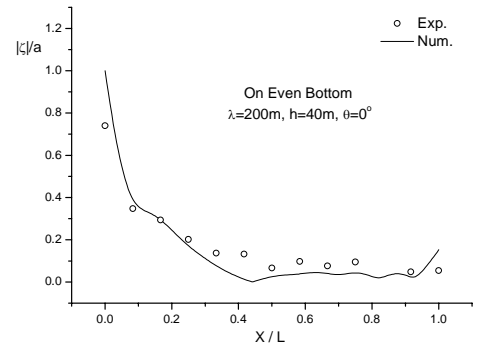
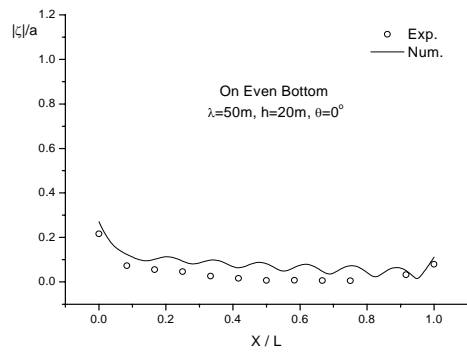


Figure 4 Hydroelastic responses of VLFS on even bottom

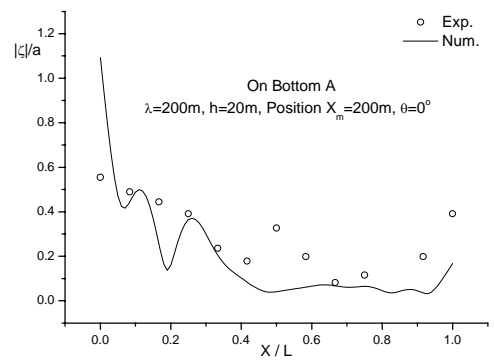
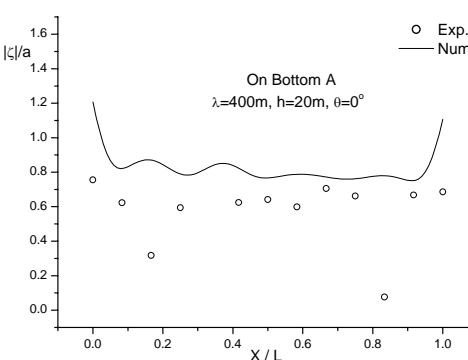
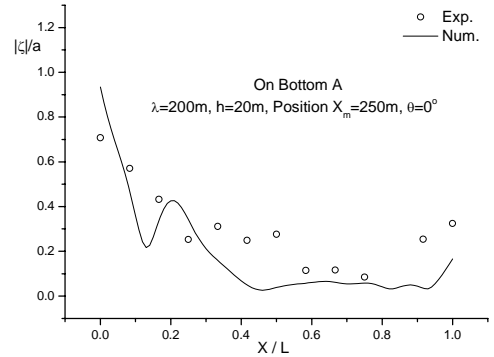
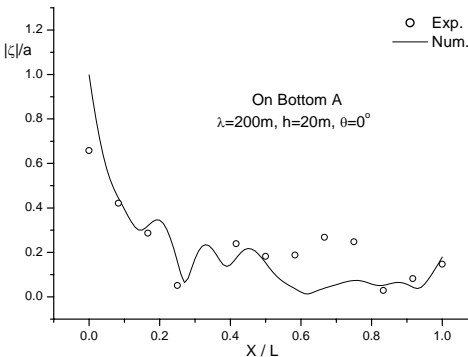
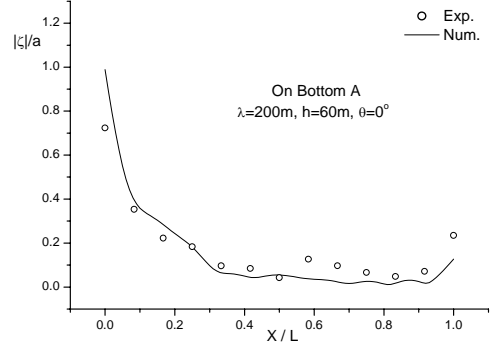
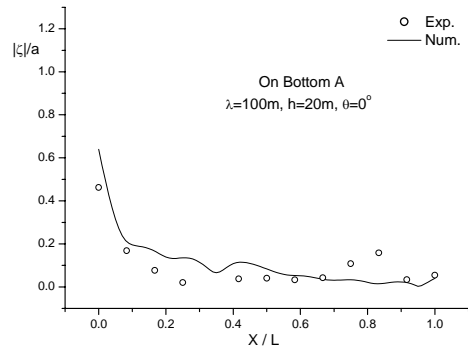
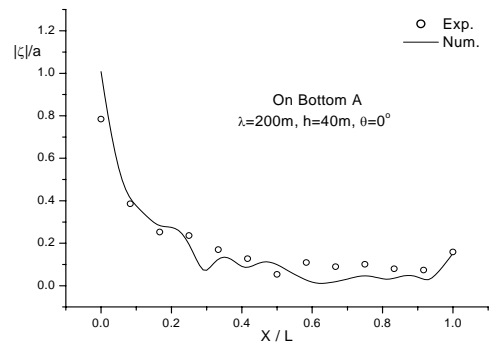
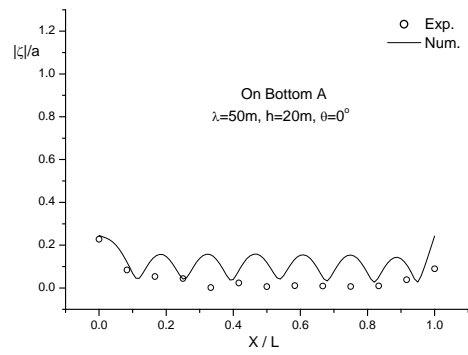


Figure 5 Hydroelastic responses of VLFS on bottom A

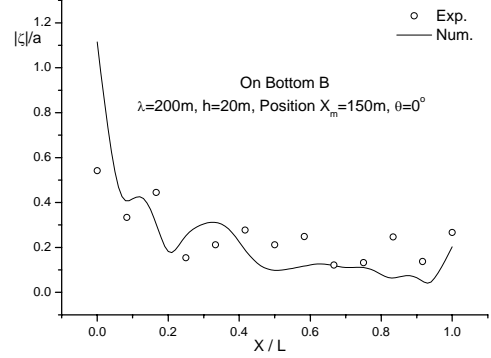
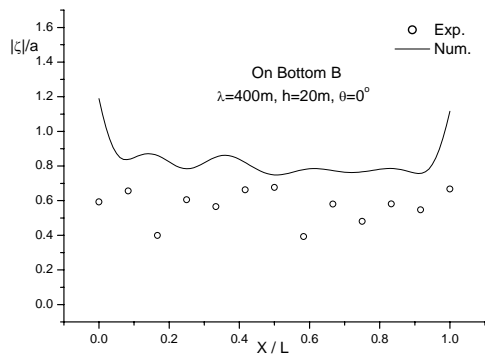
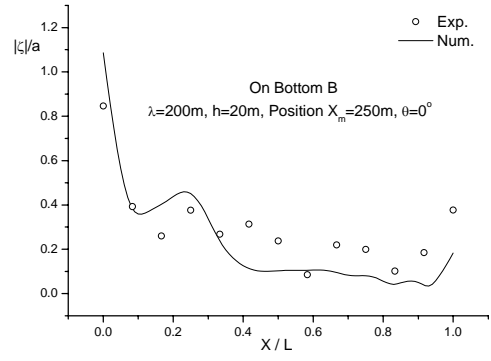
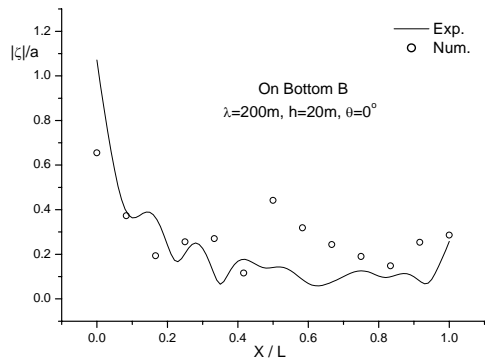
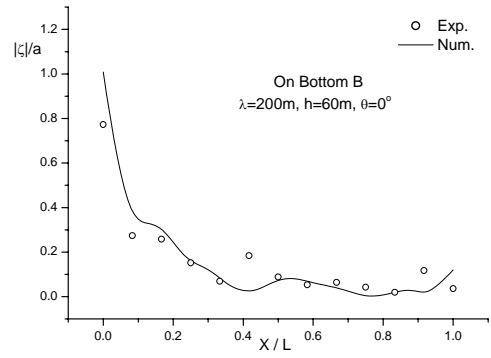
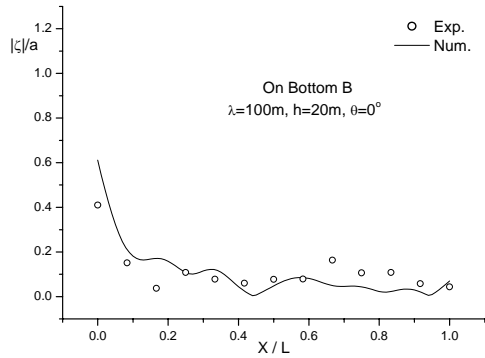
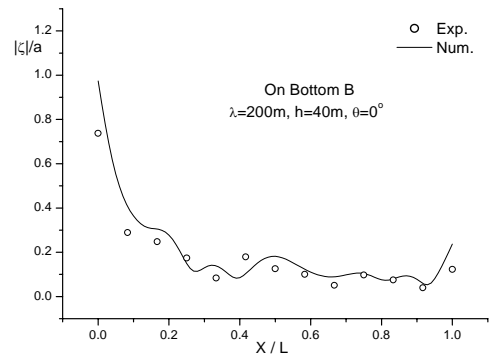
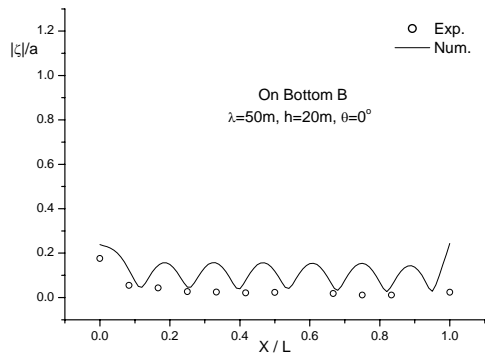


Figure 6 Hydroelastic responses of VLFS on bottom B

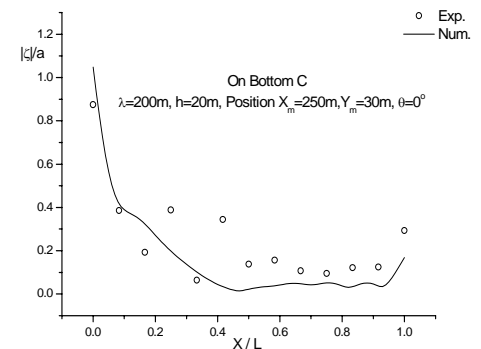
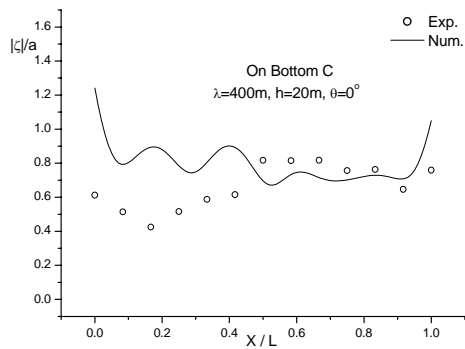
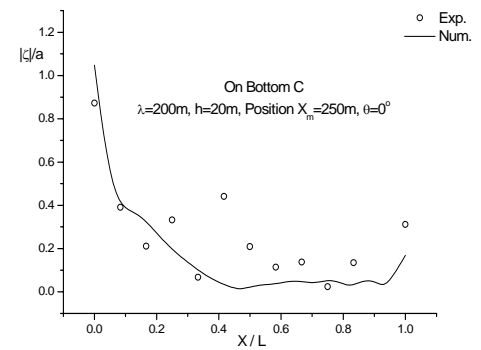
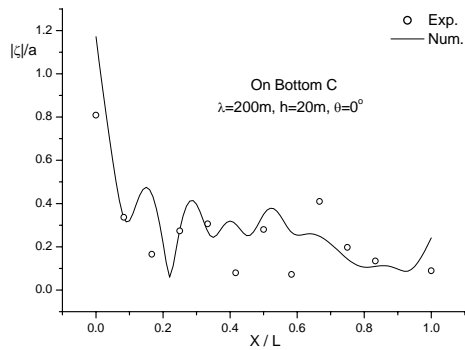
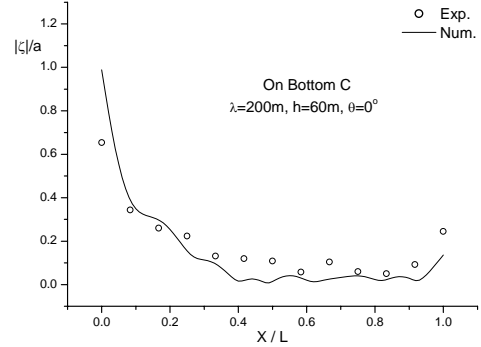
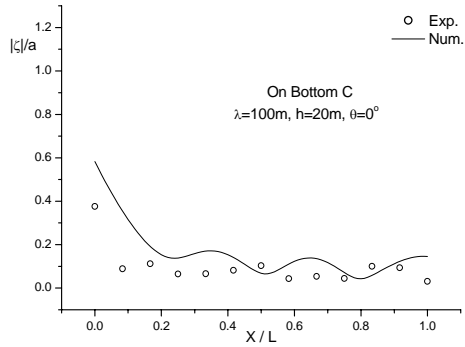
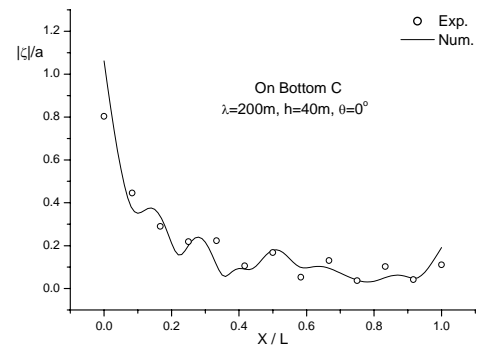
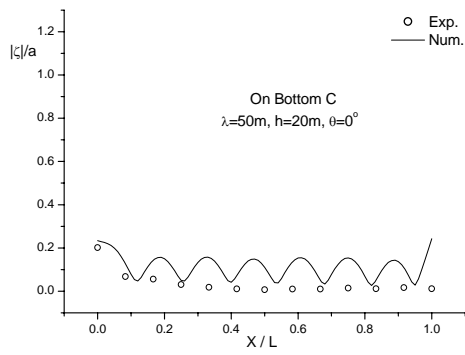


Figure 7 Hydroelastic responses of VLFS on bottom C

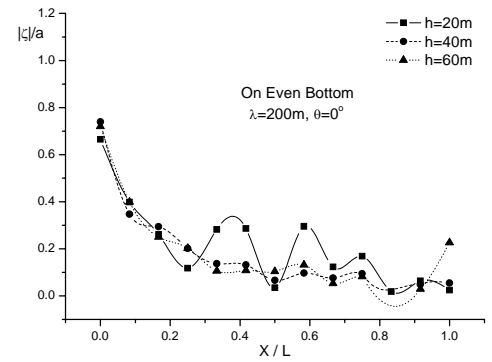
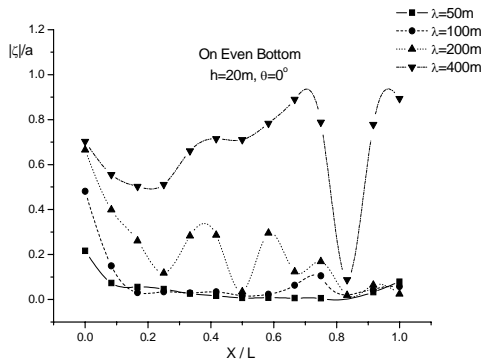
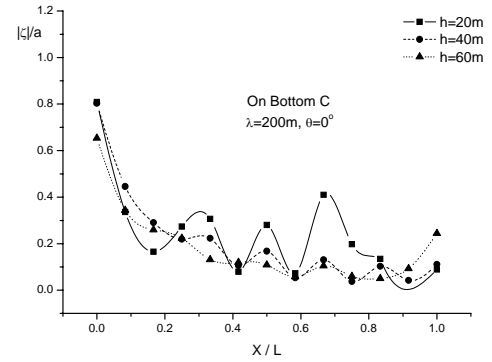
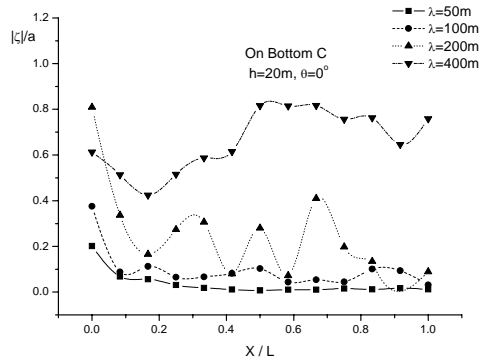
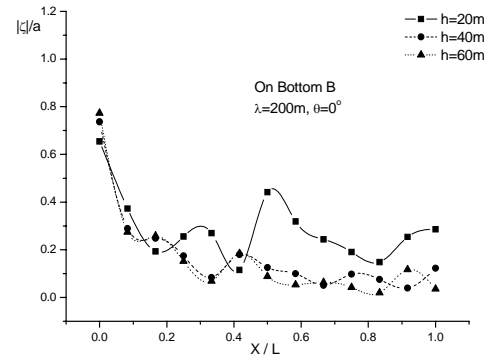
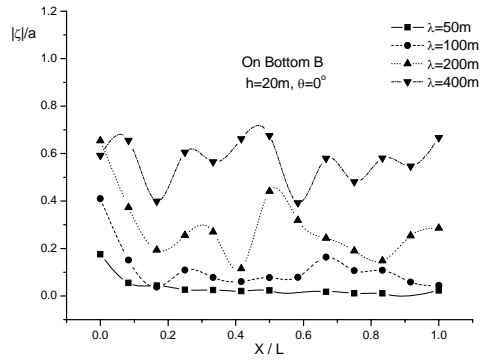
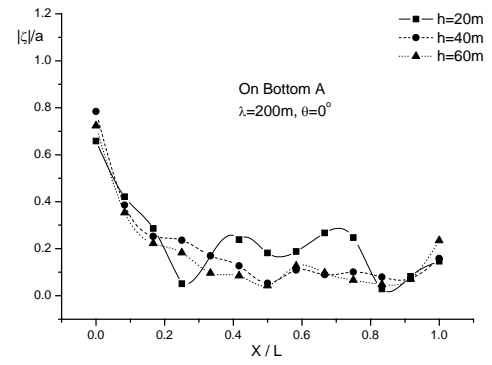
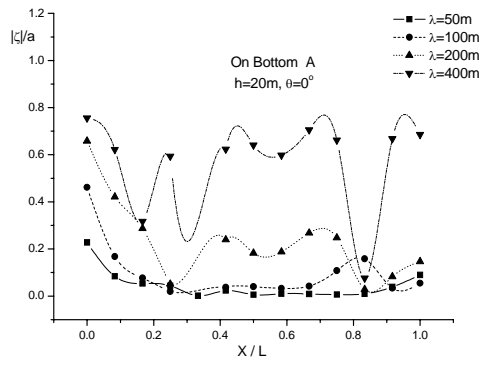


Figure 8 Effect of wavelength on centreline deflection of VLFS on different bottoms

Figure 9 Effect of water depth on centreline deflection of VLFS on different bottoms

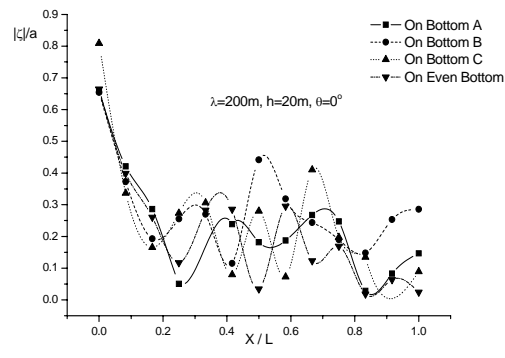
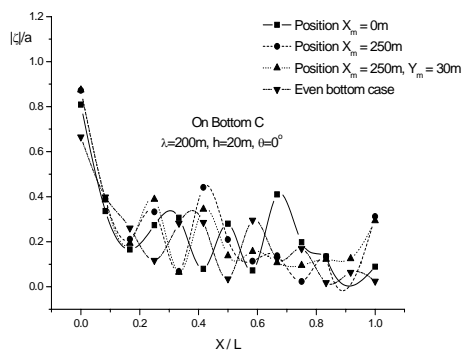
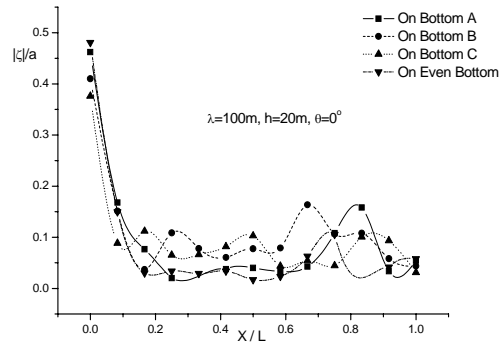
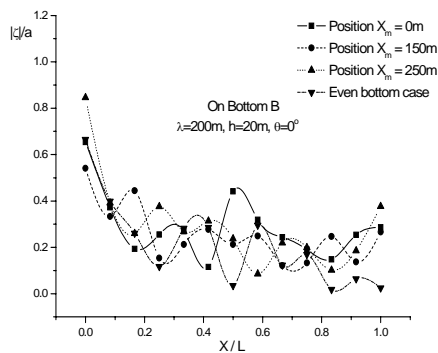
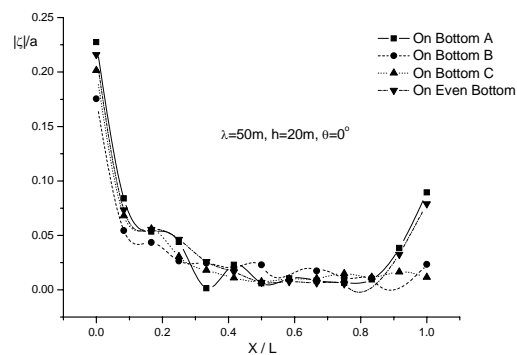
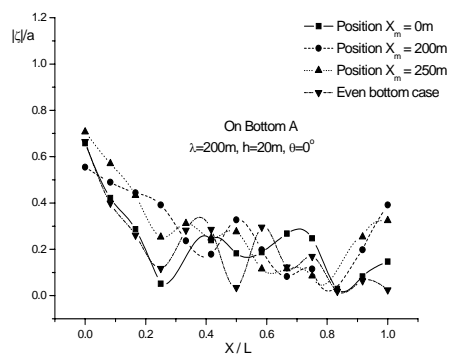


Figure 10 Effect of shoal position on centreline deflection of VLFS in inhomogeneous environment

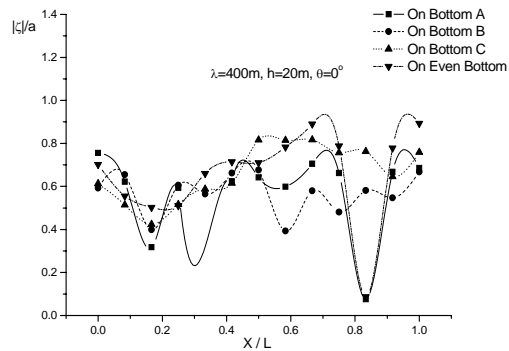


Figure 11 Effects of wavelength and different bottoms on the deflection of VLFS

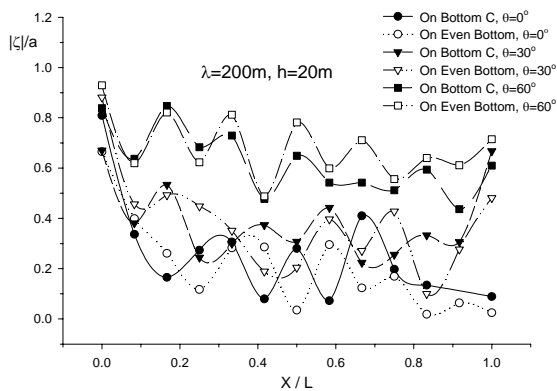


Figure 12 Effects of incident angle on the deflection of VLFS on bottom C and even bottom

SUMMARY AND CONCLUSIONS

The effect of inhomogeneous sea environment due to the variation of water depth on the hydroelastic response of VLFS is studied in this paper. The numerical method adopted in the paper is proved to be applicable to solve the problem of hydroelastic response of VLFS on uneven bottom. However, as $U_p > 1$ or the slope of the bottom becomes abrupt, the problem becomes nonlinear. The numerical method based on linear theory is no longer applicable and a nonlinear model is required. It is found that influence of the inhomogeneous sea environment in the form of uneven sea bottom is more significant in shallow water. The effect of variational water depth on plate deflection decreases as water depth increases. The effect of variational water depth on plate deflection increases as wavelength increases. It is demonstrated that the influence of the uneven sea bottom is limited to local area. It is also found that considerable larger deflections in oblique waves than that in head seas, while the effect of variational water depth decreases.

ACKNOWLEDGMENTS

This paper is based on work funded in part by National Natural Science Foundation of China (50039010) and the Science and Technology Development Foundation of Shanghai Municipal Government (00XD14015). Additional support was provided by Australia Research Council (ARC) under Grant No. DP0450906. We would like to thank the cooperation from the state key laboratory of ocean engineering in Shanghai Jiao Tong University.

REFERENCES

1. Bai, K.J., Yoo, B.S., and Kim, J.W., 2001, "A localized finite-element analysis of a floating runway in a harbor", *Marine Structures*, Vol. 14, No. 1-2, pp. 89-102.
2. Isobe, E., "Research and development of Mega-Float", 1999, *Proc. of the 3rd Int. Workshop on Very Large Floating Structures*, Vol. I, pp. 7-13.
3. Miyajima, S., Seto, H. and Ohta, M., 2002, "Hydroelastic Responses of the Mega-Float Phase-II Model in Waves", *Proc. 12th Int. Offshore Polar Eng. Conf.*, Vol. II, pp.298-304.
4. Takagi, K. and Kohara, K., 2000, "Application of the ray theory to hydroelastic behaviour of VLFS", *Proc. 10th Int. Offshore Polar Eng. Conf.*, Vol. I, pp.72-77.
5. Taylor, R.E. and Ohkusu, M., 2000, "Green functions for hydroelastic analysis of vibrating free-free beams and plates", *Applied Ocean Research*, Vol. 22, No.5, pp. 295-314.
6. Utsunomiya, T., Watanabe, E. and Nishimura, N., 2001, "Fast multipole algorithm for wave diffraction/radiation problems and its application to VLFS in variable water depth and topography", *Proc. 20th Int. OMAE Conf.*, CD-ROM: OMAE01/OSU-5202.
7. Wang, C.D. and Meylan, M.H., 2002, "The linear wave response of a floating thin plate on water of variable depth", *Applied Ocean Research*, Vol. 24, No. 3, pp.163-174.
8. Webster, W.C., 2000, "Mobile Offshore Base (MOB): Some structural considerations", *Proc. of the ISSC 2000 Pre-Congress Symposium on Advances in Marine Structures*.
9. Wu, Y.S., 1984, "Hydroelasticity of Floating Bodies", PhD thesis, Brunel University, UK.
10. Yan, H.M., Cui, W.C. and Liu, Y.Z., 2003, "Hydroelastic analysis of very large floating structures using plate Green functions", *China Ocean Engineering*, Vol. 17, No. 2, pp.151-162.